Thrombosis Research 182 (2019) 116–123

Contents lists available at ScienceDirect

Thrombosis Research

journal homepage: www.elsevier.com/locate/thromres

Full Length Article

Collateral vein dynamics in mouse models of venous thrombosis: Pathways consistent with humans

Olivia R. Palmer[a,*], Grey G. Braybrooks[a], Amos A. Cao[a], Jose A. Diaz[b], Joan M. Greve[a]

[a] Department of Biomedical Engineering, University of Michigan, Ann Arbor, MI 48104, United States of America
[b] Division of Surgical Research, Surgical Sciences, Vanderbilt University Medical Center, Nashville, TN 37232, United States of America

ARTICLE INFO

Keywords:
Collateral vessels
Deep vein thrombosis
MRI
Mouse models
Venogenesis

ABSTRACT

Introduction: Prolific collateralization in the venous system has been associated with more severe disease. However, there is a scarcity of information on venogenesis and collateral vessel progression over time. Further, little is understood regarding the relevance of the most common preclinical model—the mouse—for studying venous collateralization. The purpose of this work was to non-invasively and quantitatively characterize collateral vein development and progression in two murine models of deep vein thrombosis using magnetic resonance imaging (MRI).

Methods: Venous thrombosis (VT) was induced in 12–14-week-old male C57BL/6 mice using either the inferior vena cava (IVC) ligation model (n = 5) or the electrolytic IVC model (n = 5). Magnetic Resonance Imaging (MRI) methods optimized for small venous imaging were used on days 2, 6, 14, and 21 following venous thrombosis induction to quantify collateral development and thrombus volume.

Results: Collateral veins ~150–200 μm in diameter could be tracked in three dimensions. Collateral pathways were influenced by pre-existing anatomy; mice with bilateral IVC branches showed a predominant superficial collateral pathway (superficial and internal epigastric veins), whereas mice with no lateral branches exhibited a strong intermediate collateral pathway (gonadal and periureteric veins) and were less likely to develop ascending lumbar collaterals. The degree of venogenesis showed a positive correlation with thrombus volume in both models (combined $R^2 = 0.64$, $p < 0.0001$).

Conclusions: Venous collateral pathways in C57BL/6 mice are consistent with those described in humans. Collateral pathways are influenced by pre-existing anatomy, and the degree of collateralization correlates with thrombus volume.

1. Introduction

Vascular obstruction creates physical forces that promote the remodeling of pre-existing arterioles/arteries or venules/veins known as arteriogenesis and venogenesis, respectively. While arteriogenesis and therapies augmenting collateral arterial flow restore function in cases such as peripheral artery disease [1] and cerebral ischemia [2], collateral veins do not have valves and cannot fully compensate for impaired venous function [3]. As such, while prolific arterial collateralization reduces clinical symptoms, excessive venous collaterals are unable to restore function [3,4] and indicate more severe disease [5,6]. Additionally, when venous obstruction is treated by stenting, competitive flow in large collaterals increases the risk of thrombotic stent occlusion [4], making collateral size assessment an important consideration for stenting procedures.

Four collateral pathways resulting from vena cava obstruction in humans have been identified [7–10]. The deep pathway is the most common, involving enlargement of the azygos-hemiazygos system and/or ascending lumbar veins. The intermediate pathway involves the gonadal and periureteric veins, which drain into the renal veins or inferior vena cava (IVC), and is most common in humans with occlusion in the infrarenal segment of the IVC [7,11–13]. The superficial pathway involves the superficial and internal epigastric veins, which originate from the femoral and iliac veins and drain into the cephalic and brachiocephalic veins, respectively. Lastly, the portal collateral pathway is made of several subtypes identified following portal obstruction or hypertension.

Unlike arteriogenesis, venogenesis is poorly understood in part due

Abbreviations: MOTSA, multiple overlapping thin slab acquisition; TOF, time of flight; VT, venous thrombosis; IVC, inferior vena cava; EIM, electrolytic inferior vena cava model; TR, repetition time; TE, echo time; FOV, field of view; NEX, number of excitations; CNR, contrast to noise ratio

* Corresponding author at: Bonisteel Interdisciplinary Research Building, 2360 Bonisteel Blvd, Ann Arbor, MI 48109, United States of America.
E-mail address: opalmer@umich.edu (O.R. Palmer).

https://doi.org/10.1016/j.thromres.2019.08.018
Received 16 May 2019; Received in revised form 29 July 2019; Accepted 17 August 2019
Available online 23 August 2019

to a paucity of preclinical studies. Collateral veins have been briefly noted but not investigated in a porcine model of venous thrombosis (VT) [14] and a rat model of varicose veins [15]. A retrospective study of dogs with caudal IVC obstruction found collateral pathways similar to those reported in humans [11]. Additionally, a non-human primate study of ilio-femoral VT showed collateral veins persistent through day 21 in the control group but absent in treatment and prophylaxis groups [16]. However, little is understood regarding how collaterals are influenced by pre-existing anatomy or they evolve over time. Further, there is a lack of information regarding the relevance of the most common preclinical model—the mouse—for studying venous collaterals.

MRI has been used to examine collateral vessels both clinically [4,17,18] and in preclinical models [16,19]. Non contrast-enhanced angiography is increasingly desirable as safety concerns of gadolinium-based contrast agents have risen [20–22]. Time-of-flight (TOF) MRI is a commonly used non contrast-enhanced angiography method that relies on the movement of blood to achieve bright signal from patent vessels and can be performed as a 2D or 3D acquisition. A more specialized TOF method called multiple overlapping thin slab acquisition (MOTSA) reduces signal saturation while maintaining good contrast to noise ratios (CNR) between vessels and nearby stationary tissue [23,24], enabling visualization of even small collateral vessels over large extents. The purpose of this work was to quantify collateral vein development and progression in two murine models of deep vein thrombosis using MRI methods optimized for small vessel imaging.

2. Materials and methods

All experiments were approved by the University of Michigan Institutional Animal Care and Use Committee in accordance with the National Institutes of Health guide for the care and use of laboratory animals. 12–14-week-old male C57BL/6 mice weighing 27 ± 2 g were used.

2.1. Mouse models

Two models of VT were used to represent total or partial venous occlusion. Mice were anesthetized using 2% isoflurane, placed on a heating pad and a laparotomy was performed. The intestines were exteriorized and placed between saline-soaked gauze pads. In the total occlusion cohort, VT was induced by IVC ligation immediately distal to the left renal vein using 7–0 Prolene (Ethicon, Inc., Somerville, NJ), including ligation of any lateral branches (gonadal veins, which vary anatomically in their joining point with the IVC) and cauterization of both posterior (lumbar) branches that drain into the IVC in the segment between the left renal vein and the iliac bifurcation [25–29]. In the partial occlusion cohort, VT was induced using the electrolytic IVC model (EIM), which produces ~80% occlusion while maintaining blood flow [30–33]. For EIM procedures, the stripped end of a 30G copper wire (approximately 3 mm exposed length, KY- 30- 1- GRN, Electrospec, Dover, NJ) was placed in the blunted end of a 25G needle cut to 5 mm in length. Following ligation of any lateral branches, the needle with copper wire was inserted into the IVC just proximal to the iliac bifurcation, and a second wire was inserted subcutaneously to complete the circuit. A constant current of 250 μA was applied for 15 min, releasing free radicals in the copper wire and activating endothelial cells within the IVC [33]. Following needle removal, the muscle was closed with continuous sutures using 5-0 Vicryl (Ethicon, Inc., Somerville, NJ), and the skin with Vetbond (3 M, St. Paul, MN, USA). A more detailed description of both surgical procedures can be found in Diaz et al. [34].

Analgesics were not used for these surgical procedures as analgesics are proven to introduce confounding variables in studies of venous thrombosis [35]. Our veterinary group showed that many analgesics interfere negatively with the natural history of thrombosis formation and development processes, affecting thrombus size while also altering the associated inflammatory process [35]. As such, all of our mouse thrombosis studies have received an IACUC-approved exemption from analgesics. Animals were typically active—eating, drinking and grooming—within minutes following the surgery, and were monitored daily.

2.2. MRI

Imaging was performed at 7 Tesla (Agilent Technologies, Santa Clara, CA) using a 40 mm volume coil (Morris Instruments, Ontario, Canada). Mice were anesthetized with 2% isoflurane. Respiration was monitored and maintained at 60–100 breaths/min (SA Instruments, Inc., NY). A proportional-integral-derivative controller maintained the animal's temperature at 37 ± 1 °C via warm air circulation. Mice were imaged at days 2, 6, 14 and 21 post VT induction, with a mean total imaging time of 1.25 h.

The number of collateral vessels and their respective pathways were quantified using 3D TOF MOTSA: FOV: 34 × 34 × 17 mm, matrix: 128 × 128 × 64 zero-filled to 256 × 256 × 128, isotropic resolution $(132\,\mu m)^3$, radiofrequency excitation thickness: 6 mm, TR/TE: 30/2.84 ms, FA 25°, NEX 2, 8 slabs with 50% overlap, imaging time 3 m 25 s per slab with a total of 8 slabs. These final parameters resulted from balancing the primary goal of a high CNR between vessels and nearby stationary tissue in order to track collaterals over large extents with minimized acquisition time due to repeated imaging. Using an in-house MATLAB script, thin slabs were overlapped and aligned using the spatial coordinates of each dataset (Mathworks; Natick MA). In areas of overlap between two adjacent thin slabs, voxel pairs were evaluated and the highest intensity voxel was assigned to the final volume. 3D volumetric renderings of the MOTSA were used to count and classify collateral pathways based on location. The merged single continuous 3D volume enabled visualization of collateral vessels ~150–200 μm in diameter. A separate naïve mouse was imaged at higher resolution to demonstrate the baseline pre-surgical anatomy by MRI (FOV: 38 × 38 × 30, matrix: 256 × 256 × 128 zero-filled to 512 × 512 × 256, resolution 148 μm × 148 μm × 234 μm, radiofrequency excitation thickness: 6 mm, TR/TE: 30/2.84 ms, FA 25°, NEX 2).

To assess thrombus volume, 2D TOF axial slices were acquired from the renal vessels to the iliac bifurcation (20 contiguous slices, each 1 mm thick; TR/TE: 15/4.9 ms, FA 20°, FOV: $(30\,mm)^2 \times 30$ mm, matrix 256 × 256 zero-filled to 512 × 512, in-plane resolution $(58.6\,\mu m)^2$, NEX: 3, 3 m 50 s). Thrombus volume was assessed by manual segmentation of no-flow regions within the IVC (i.e. low signal intensity on TOF MRI; MRVision, Winchester, MA). Higher resolution imaging was used to quantify thrombus volume because of the need to rely on low signal intensity which can be more challenging to distinguish from surrounding tissue.

Cross-sectional areas of the IVC prior to thrombus induction and of all collateral veins following thrombus induction were quantified and summed at a slice 6 mm proximal to the iliac bifurcation (the approximate midpoint of the thrombus) using 2D axial TOF MRI. To distinguish venous flow, acquisitions with saturation bands to null arterial (proximal band) or venous (distal band) flow were used (TR/TE: 20/4.9 ms, FA 20°, FOV: $(30\,mm)^2$, matrix: 256 × 256 zero-filled to 512 × 512, in-plane resolution: $(58.6\,\mu m)^2$, NEX: 6, saturation band thickness 5 mm placed directly adjacent to the acquisition slice, imaging time 30 s). Using a saturation band to null signal from arterial flow results in any bright signal remaining in the image being derived solely from venous flow and allows automatic segmentation (using thresholding) because arteries that might be closely juxtaposed to veins are no longer visible.

2.3. Statistical analysis

Data were analyzed using GraphPad Prism version 8.0 (GraphPad

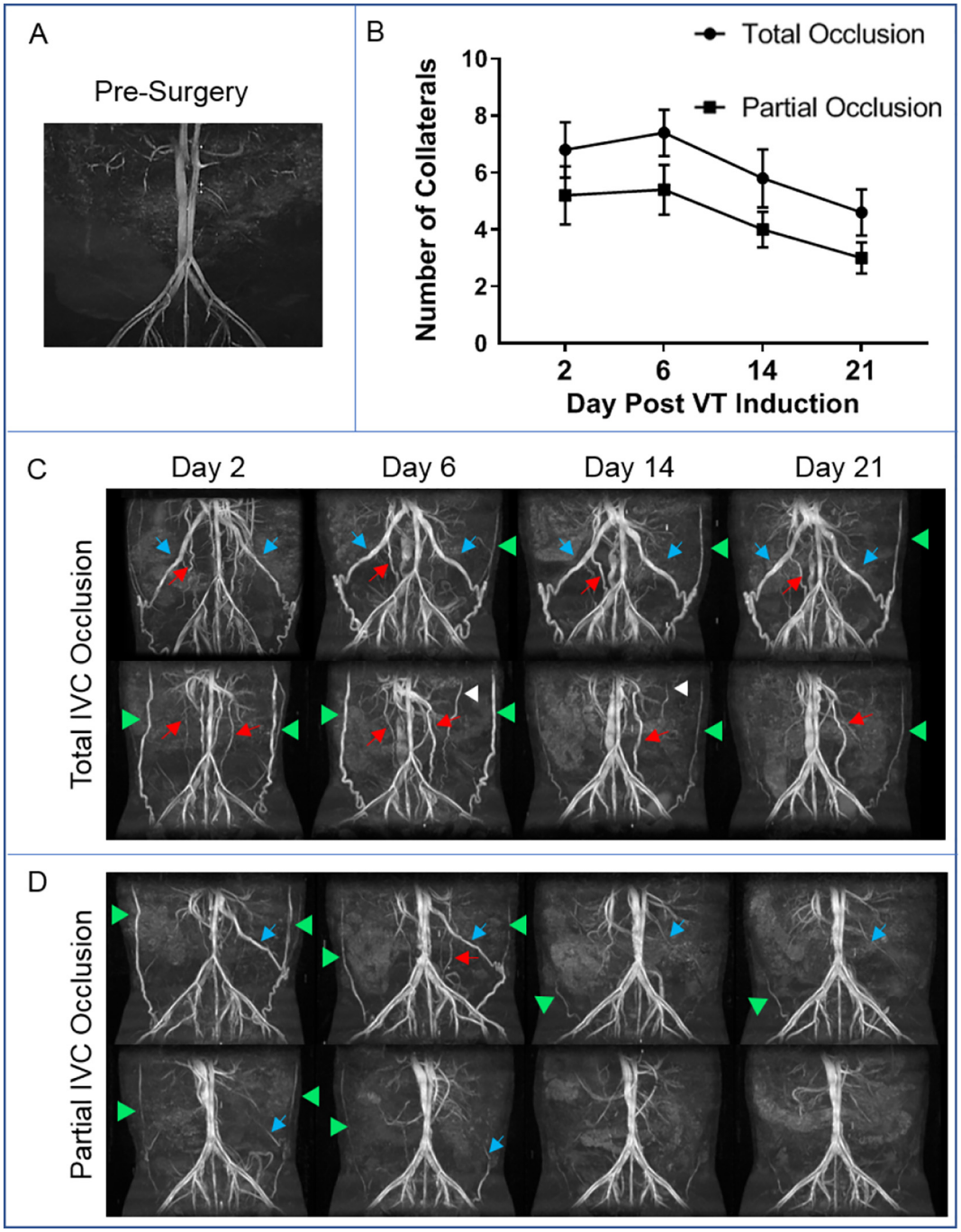

Fig. 1. A) Coronal maximum intensity projections (MIPs) from MOTSA from a naïve mouse demonstrating the baseline vasculature. B) Number of collateral veins over time in two models of caval thrombosis. C & D) Representative coronal MIPs from MOTSA acquired at days 2, 6, 14, and 21 for two animals from each of the models used: C) inferior vena cava ligation (total IVC occlusion) or D) electrolytic induced IVC stenosis (partial IVC occlusion). Green arrowheads: superficial epigastric veins; white arrowheads: internal epigastric veins; blue arrows: gonadal veins; red arrows: periureteric veins. Ascending lumbar veins not visible in coronal images. The aorta and iliac arteries are present in all images. (For interpretation of the references to color in this figure legend, the reader is referred to the web version of this article.)

Software, La Jolla, CA). A repeated measures one-way ANOVA was used to compare collateral numbers and cross-sectional area across time points within each model. An unpaired two-tailed *t*-test was used to compare the two models. A linear regression was performed on total cross-sectional collateral area vs. thrombus volume for both models to determine whether the slopes were significantly different from zero. ANCOVA was used for comparisons between linear regression fits between models. All data are plotted as mean ± standard error. Significance was set at $p < 0.05$.

3. Results

3.1. MOTSA allows quantification of collateral vein pathways in vivo

3D renderings of the volume enabled tracking of collateral vessel pathways (Movie 1). Extraperitoneal collaterals showed a tortuous pattern, whereas gonadal and superficial epigastric veins took a nearly straight path (Fig. 1, green arrowheads and blue arrows, respectively). Internal epigastric and periureteral collaterals showed a corkscrew

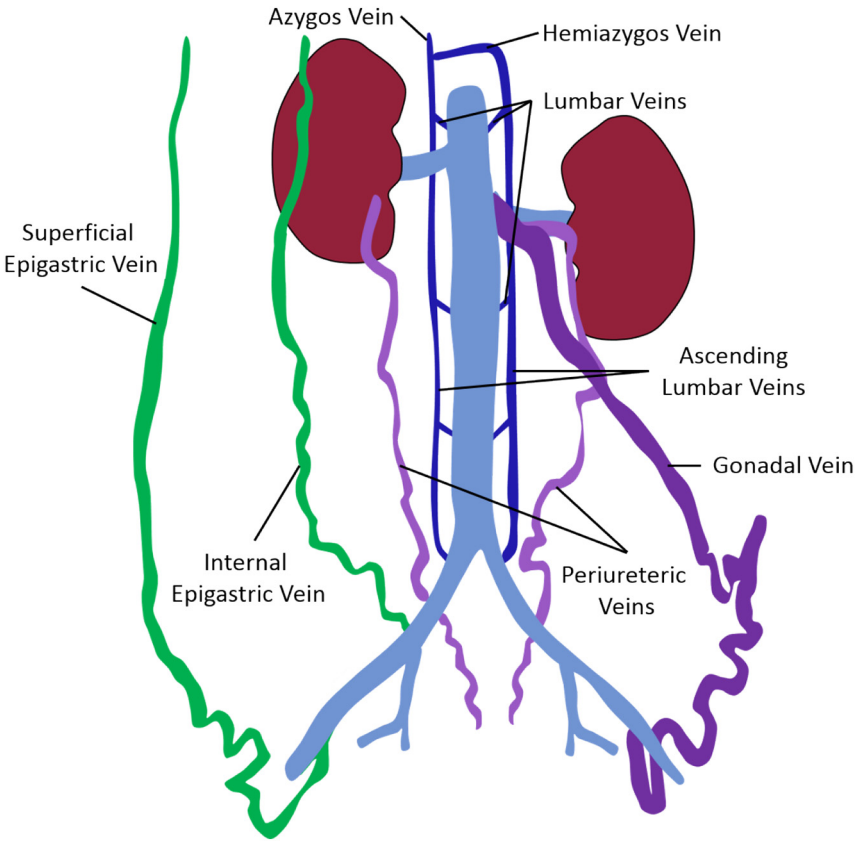

Fig. 2. Schematic representation of the superficial (green), intermediate (purple), and deep (dark blue) collateral vein pathways in C57BL/6 mice following inferior vena cava obstruction. (For interpretation of the references to color in this figure legend, the reader is referred to the web version of this article.)

pattern (Fig. 1A–B, white arrowheads and red arrows, respectively).

Collateral vessels were most prominent at early time points following thrombus induction (Fig. 1C). In both models, the number of collaterals peaked at day 6, although none of the time points studied were significantly different from one another (total occlusion—D2: 6.8 ± 0.9, D6: 7.4 ± 0.8, D14: 5.8 ± 1.0, D21: 4.6 ± 0.8; partial occlusion—D2: 5.2 ± 1.0, D6: 5.4 ± 0.9, D14: 4.0 ± 0.6, D21: 3.0 ± 0.5). While total vessel occlusion had more collateral vessels compared to partial occlusion at every time point, there was no significant difference in total number of collaterals between the models.

Three of the four collateral vein pathways described in humans were observed in mice (Fig. 2). Both models exhibited the deep, intermediate, and superficial collateral pathways (Fig. 3). Deep collaterals (ascending lumbar veins, Fig. 3B, black arrowhead) were observed in 4/5 total occlusion and 3/5 partial occlusion mice, most commonly rejoining the IVC via a lumbar vein proximal to the thrombus (Fig. 3B, white arrowhead). Interestingly, for mice in the partial occlusion cohort exhibiting ascending lumbar collaterals, this deep collateral pathway persisted across time points, whereas in the total occlusion cohort only one of the three mice with the deep collateral pathway continued to show visible ascending lumbar collaterals beyond day 2 (Fig. 3A). The intermediate collateral pathway was observed in all mice (Fig. 3C). The superficial collateral pathway, also observed in all mice, was more prevalent in the total occlusion model (Fig. 3E, $p < 0.05$).

3.2. Collateral pathway is influenced by pre-existing vascular anatomy

The pathways of collateral vessels showed consistent trends related to the pre-existing anatomical pattern of branching vessels draining into the IVC (Fig. 4). C57BL/6 mice have four anatomical patterns of branching vessels draining into the IVC: no branches – 21%, right branches only – 34%, left branches only – 20%, and bilateral branches – 25% [27]. Any lateral branches that drain into the IVC between the left renal vein and iliac bifurcation are interrupted during thrombus induction for both models used. Mice with no lateral branches tended to predominantly rely on the intermediate collateral pathway (Fig. 4A), whereas mice with bilateral side branches predominantly exhibited the superficial collateral pathway, with some involvement of the periureteral but not gonadal veins from the intermediate pathway (Fig. 4C). When unilateral branches were present, the side with the interrupted branch followed the superficial collateral pathway, while the contralateral side took an intermediate collateral pathway (Fig. 4B).

3.3. Total collateral cross-sectional area correlates with thrombus volume

Cross-sectional area of the IVC prior to surgery and collateral veins after surgery were measured in a slice 6 mm proximal to the iliac bifurcation (the midpoint of the thrombus) from axial TOF MRI using thresholding. Pre-surgical IVC cross-sectional areas for the total and partial occlusion cohorts were $0.88 \pm 0.24\,mm^2$ and $0.89 \pm 0.24\,mm^2$, respectively. As shown in Fig. 5A–C, a saturation band placed first proximal then distal to the slice of interest was used to verify venous flow for measurements of collateral veins. Cross-sectional area of collateral vessels following total IVC occlusion was more than double that of partial occlusion (Fig. 5D, D2: $2.3 \pm 0.6\,mm^2$ total occlusion vs. $0.8 \pm 0.4\,mm^2$ partial occlusion, D6: $2.5 \pm 0.6\,mm^2$ total occlusion vs. $0.8 \pm 0.3\,mm^2$ partial occlusion, D14: $1.2 \pm 0.5\,mm^2$ total occlusion vs. $0.4 \pm 0.2\,mm^2$ partial occlusion, D21: $1.1 \pm 0.5\,mm^2$ total occlusion vs. $0.2 \pm 0.1\,mm^2$ partial occlusion, total vs. partial occlusion overall $p < 0.05$). The cross-sectional area of collateral veins peaked at day 6 following thrombus induction in both models. In the total occlusion cohort, cross-sectional area of collaterals at days 14 and 21 were significantly smaller than at day 6 ($p < 0.01$). In the partial occlusion cohort, cross-sectional area of collaterals at day

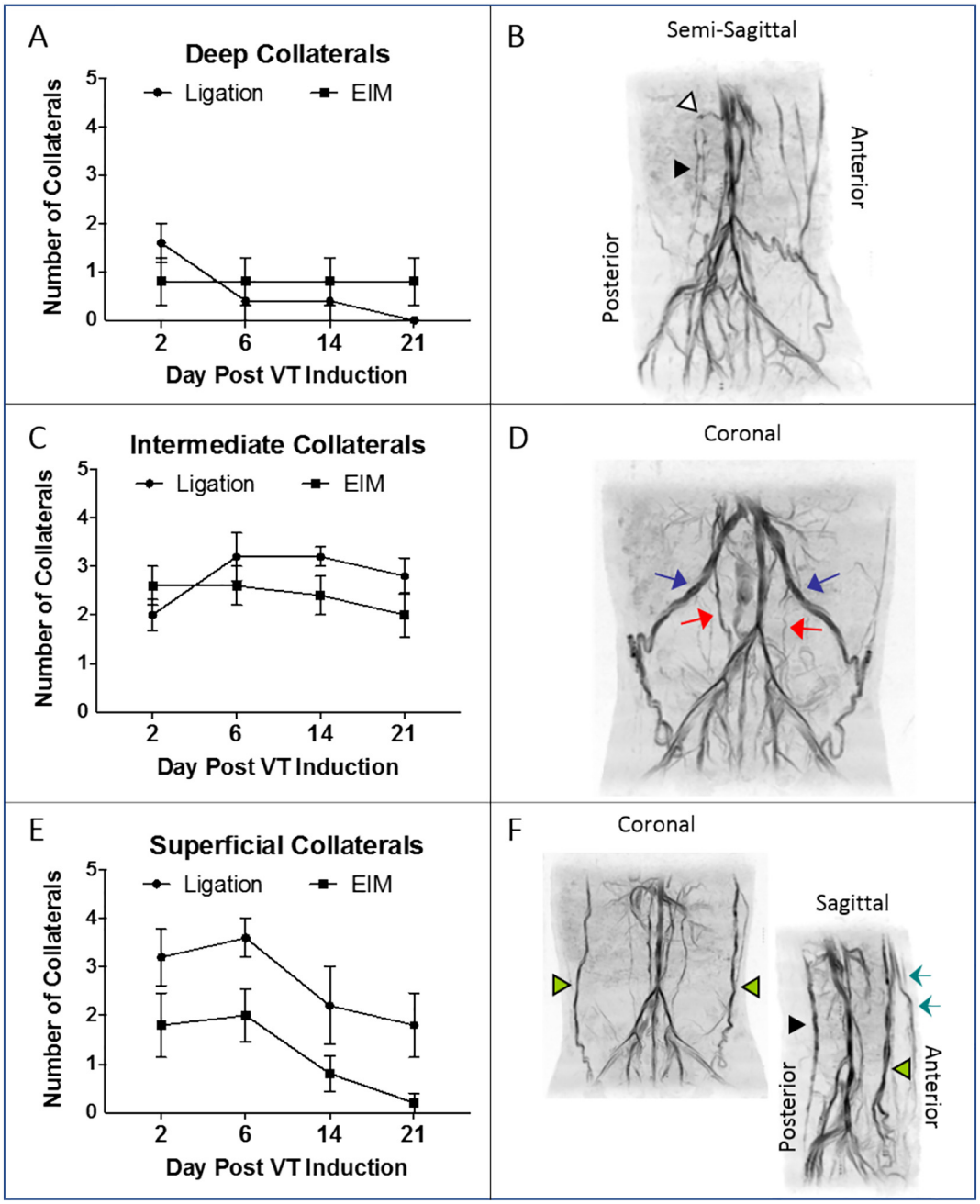

Fig. 3. Number of collaterals in each pathway with corresponding MOTSA data, inverted color scale for clarity: deep collaterals (A), ascending lumbar veins noted by black arrowhead, white arrowhead denoting the rejoining with the IVC through the lumbar vein (B); intermediate collaterals (C) with gonadal (blue arrows) and periureteral (red arrows) veins (D); and superficial collaterals (E) with superficial (green arrowheads) and internal (teal arrows) epigastric veins (F). (For interpretation of the references to color in this figure legend, the reader is referred to the web version of this article.)

21 was significantly smaller than at day 6 ($p < 0.05$).

In both VT models, the thrombus naturally resolves over time, with peak thrombus burden at day 2 [34]. To determine whether the blood volume diverted to collateral vessels correlated with the degree of IVC obstruction at the same time point, a linear regression of collateral cross-sectional area vs. thrombus volume from both models across time points was performed (Fig. 6). The sum of cross-sectional area from all collaterals at the midpoint of the thrombus showed a significant correlation with thrombus volume in both models, with no significant difference between total or partial occlusion models (total IVC occlusion: $R^2 = 0.53$, $p < 0.01$, partial IVC occlusion: $R^2 = 0.3$, $p < 0.05$, combined $R^2 = 0.64$, $p < 0.0001$).

4. Discussion

Using two well-established models of VT, we have non-invasively quantified the endogenous dynamic response to IVC thrombosis using MRI optimized to visualize and quantify collateral veins. Three of the four collateral pathways previously reported in humans were observed in mice. As in humans, the degree of collateralization correlated with the severity of obstruction [4,5]. The total stasis model had more and larger collateral vessels at all time-points compared to partial occlusion. In mouse models of VT, thrombus size peaks at day 2 and then gradually decreases as the thrombus resolves and IVC blood flow is restored. The number and size of collateral vessels parallels the thrombus resolution process, with decreasing collateral presence at days 14 and

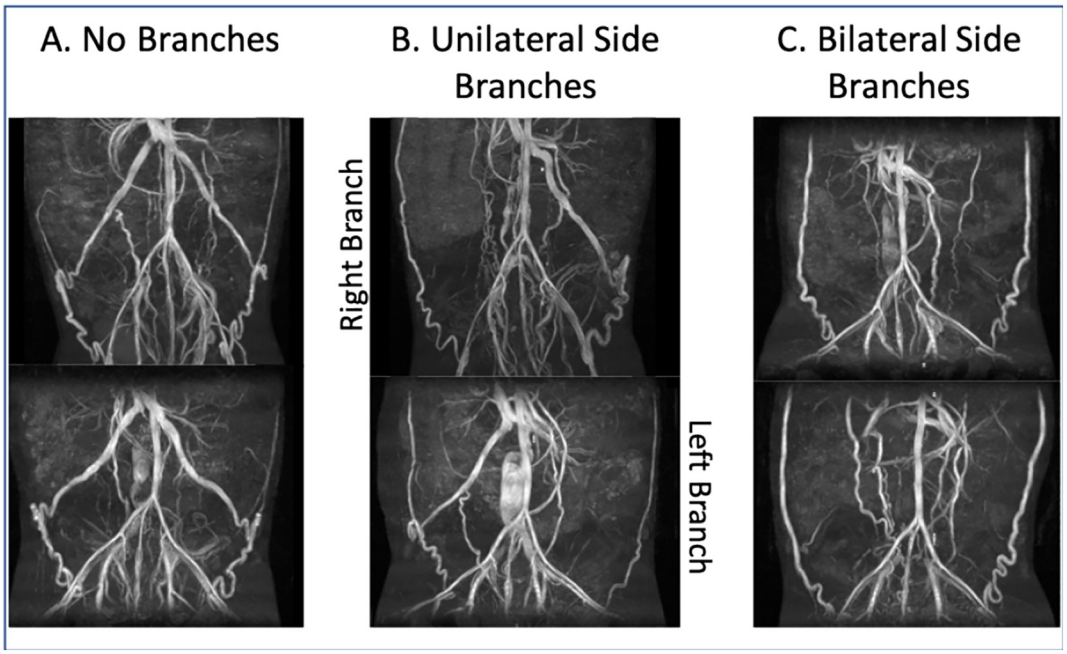

Fig. 4. Representative coronal maximum intensity projections from MOTSA showing collateral vessel pathways in mice 6 days post thrombus induction (total occlusion cohort) grouped by anatomical patterns of pre-existing branches draining into the IVC, which are interrupted during thrombus induction.

21. However, the presence of a thrombus permanently alters the vein wall, leading to increased vein wall intimal thickness and fibrosis [26]. Thus, restoration of flow attenuates collateral presence but does not eliminate it; at least 2 collateral vessels continued to be visible through day 21 in all mice.

Interestingly, the peak collateral cross-sectional area following total IVC obstruction was more than double that of pre-surgical IVC cross-sectional area (collaterals: $2.5 \pm 0.6\,mm^2$ vs. baseline IVC: $0.88 \pm 0.24\,mm^2$). This may be due to less efficient hemodynamics through the newly formed venous collaterals. Conversely, peak collateral cross-sectional area following partial IVC obstruction ($0.8 \pm 0.3\,mm^2$) accounted for roughly 90% of baseline IVC cross-sectional area ($0.89 \pm 0.24\,mm^2$). Importantly, collateral cross-sections were measured from an axial slice, representing a limitation in that this slice was not necessarily perpendicular to each collateral vessel. Rather than increasing imaging time by planning acquisitions perpendicular to each vein, we used signal intensity thresholding to quantify cross-sectional area, which discards lower signal intensity regions representing oblique sections of the vessel. Due to limits of resolution, there may be smaller collateral veins that remain undetected. However, other methodologies (e.g. vascular casting combined with higher resolution imaging modalities) introduce limitations related to reproducibly filling the vasculature, small field-of-view, or not being able to follow the same animal over time [36]. The initial, non-invasive quantification we have been able to provide here is important because a healthy vascular network requires a balanced combination of larger-caliber vessels acting as primary conduits, as well as smaller vessels which are integral at the tissue level.

The tortuous path of collateral vessels and the slower blood flow in veins typically makes visualization with non-contrast enhanced MR

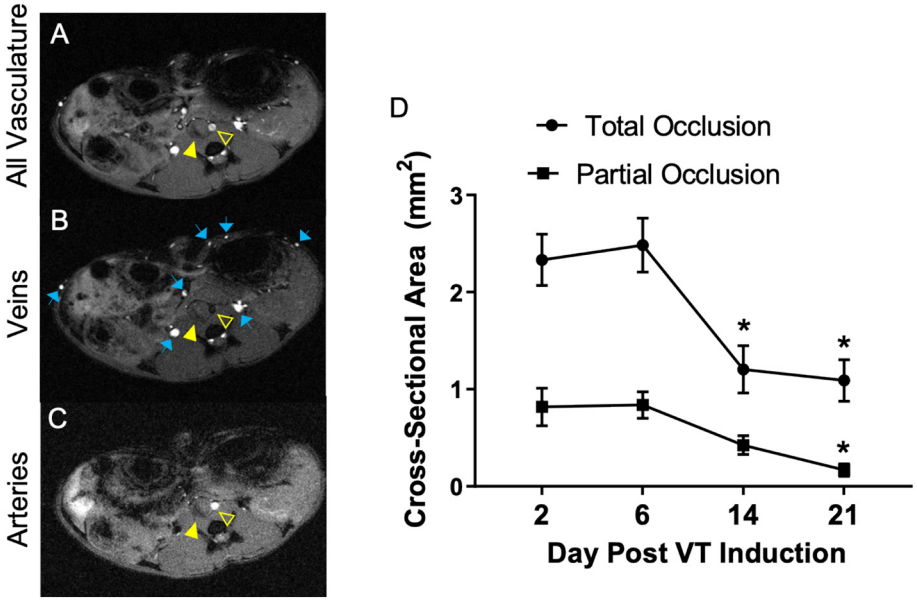

Fig. 5. Representative axial time-of-flight image showing all vasculature (A), the same slice with saturated arterial flow to show venous collaterals – blue arrows (B), and saturated venous flow to show arteries (C). (D) Collateral vein cross-sectional area from an image acquired at the midpoint of the thrombus. * denotes difference from the same model at day 6, $p < 0.05$. Filled arrowhead – thrombus; open arrowhead – aorta. (For interpretation of the references to color in this figure legend, the reader is referred to the web version of this article.)

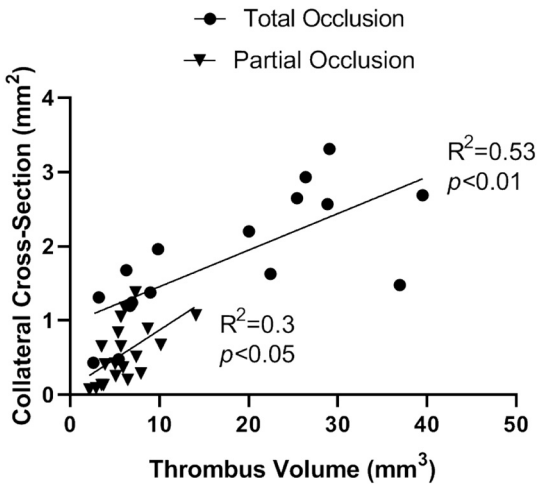

Fig. 6. Total collateral cross-sectional area correlates with thrombus volume for both the total and partial IVC occlusion models (combined $R^2 = 0.64$, $p < 0.0001$). Data is from two models of inferior vena cava thrombosis (partial or total occlusion) at days 2, 6, 14, and 21 following thrombus induction.

angiography challenging. MOTSA overcomes some of these challenges by acquiring multiple shorter fields of view and then combining them post-acquisition, enabling imaging of longer extents of blood vessels [23]. The overlapping of slabs results in venetian blind artifacts. However, our efforts to minimize these artifacts using a slab thickness of 6 mm with 50% overlap, optimizing TR and FA for venous contrast, and acquiring isometric voxels enabled us to resolve both small vessels and vessels following a tortuous path.

The deep collateral pathway was observed in 7/10 mice via enlargement of the ascending lumbar veins. However, the deep collateral pathway in mice reconnected to the IVC through a lumbar vein proximal to the thrombus in all cases rather than extending to the azygos and hemiazygos veins, a preferential collateral pathway in humans with superior vena cava obstruction [7]. C57BL/6 mice consistently have two lumbar veins draining into the IVC between the left renal vein and iliac bifurcation. These lumbar veins are cauterized in the total occlusion model, but remain patent in the partial occlusion model. As such, the deep collateral pathway presents less flow resistance in the partial occlusion cohort, which supports the observed persistence of this pathway over time in this group.

Interestingly, the deep collateral pathway was present in all mice with at least one lateral branch, whereas only 1 of 4 mice with no lateral branches exhibited deep collaterals. Likewise, mice with no lateral branches displayed less prominent superficial collaterals. In the anatomical variation with no lateral branches, the right gonadal vein connects with the IVC at or proximal to the left renal vein, while the left gonadal vein connects with the left renal vein. The gonadal veins are the largest pre-existing vessels of the collateral pathways, making venogenesis via the intermediate pathway the most prevalent when the anatomical variant did not necessitate their interruption during thrombus induction. Conversely, mice with bilateral branches (both gonadal veins draining into the IVC between the left renal vein and iliac bifurcation) displayed the most prominent superficial collaterals, persisting through day 21 under total occlusion and day 14 under partial occlusion. As expected, the portal collateral pathway was not observed in these models because the thrombus in both models does not extend beyond the renal veins, thus the portal vein was not obstructed. The phenotype of a possible portal collateral pathway in mice remains to be investigated.

Female mice were not used in this study due to an anatomical challenge in C57BL/6 females; ligation of the right uterine vein, necessary for both models as it drains into the infrarenal IVC, leads to necrosis of the reproductive organs [37]. Thus, we would not be able to humanely study chronic time points in female C57BL/6 mice. This limitation may be overcome through the use of mice from the BALBc background, which often do not have lateral IVC branches but rather increased lumbar branches. Differences in collateral numbers, pathways, and size between mouse strains and the presence and relevance of BALBc collateralization to humans remains to be investigated.

In conclusion, MOTSA enabled tracking of small tortuous veins in any anatomical plane, and revealed that collateral pathways are influenced by pre-existing anatomy. These data support that murine models are relevant tools to study venogenesis and the use of MOTSA as a tool of choice with which to study this process. Importantly, we have shown that the collateral pathways in mice are consistent with those described in humans. Also similar to humans, collateralization in mice correlates with the degree of obstruction. This work represents the first quantitative characterization of the dynamics of collateral pathways following IVC obstruction in mice, which is critical for understanding the pathophysiology in preclinical modeling. This mapping may be helpful for researchers to make observations regarding therapeutic effects, including variable therapeutic response due to inconsistencies in drug access to the thrombus for systemic therapies.

Supplementary data to this article can be found online at https://doi.org/10.1016/j.thromres.2019.08.018.

References

[1] Bondke Persson, Buschmann, Lindhorst, Troidl, Langhoff, Schulte, Buschmann, Therapeutic arteriogenesis in peripheral arterial disease: combining intervention and passive training, Vasa. 40 (2011) 177–187. doi:https://doi.org/10.1024/0301-1526/a000092.
[2] Y. Nishijima, Y. Akamatsu, P.R. Weinstein, J. Liu, Collaterals: implications in cerebral ischemic diseases and therapeutic interventions, Brain Res. 1623 (2015) 18–29, https://doi.org/10.1016/j.brainres.2015.03.006.
[3] F. Lurie, Invited commentary, J. Vasc. Surg. Venous Lymphat. Disord. 5 (2017) 95, https://doi.org/10.1016/J.JVSV.2016.06.014.
[4] T.M. van Vuuren, S. Doganci, I.M. Toonder, R. De Graaf, C.H. Wittens, Venous stent patency may be affected by collateral vein lumen size, Phlebology. 34 (2018) 32–39, https://doi.org/10.1177/0268355518755959.
[5] R.L.M. Kurstjens, T.M.A.J. van Vuuren, M.A.F. de Wolf, R. de Graaf, C.W.K.P. Arnoldussen, C.H.A. Wittens, Abdominal and pubic collateral veins as indicators of deep venous obstruction, J. Vasc. Surg. Venous Lymphat. Disord. 4 (2016) 426–433, https://doi.org/10.1016/j.jvsv.2016.06.005.
[6] W.-S. Lou, J.-P. Gu, X. He, L. Chen, H.-B. Su, G.-P. Chen, J.-H. Song, T. Wang, Endovascular treatment for iliac vein compression syndrome: a comparison between the presence and absence of secondary thrombosis, Korean J. Radiol. 10 (2009) 135, https://doi.org/10.3348/kjr.2009.10.2.135.
[7] S. Kapur, E. Paik, A. Rezaei, D.N. Vu, Where there is blood, there is a way: unusual collateral vessels in superior and inferior vena cava obstruction, RadioGraphics. 30 (2010) 67–78, https://doi.org/10.1148/rg.301095724.
[8] L.M. Orella, J.M. Mellado, N.Y. Barea, S.S. Alava, R.L. López, J.M. Cuartero, ECR 2010/C-3062/Collateral pathways of the abdominal wall: anatomical review and pathologic findings at 64-slice multidetector CT angiography, in: Eur. Soc. Radiol., 2010: pp. C–3062. doi:https://doi.org/10.1594/ecr2010/C-3062.
[9] E. Kalchev, R.D. Popova, G. Valchev, Balev B., B.G. Varna, Congenital absence of inferior vena cava, in: EPOS - ECR, 2015. https://posterng.netkey.at/esr/viewing/index.php?module=viewing_poster&task=viewsection&pi=127172&ti=438712&si=1482&searchkey= (accessed January 21, 2019).
[10] D.L.M. Oterdoom, B.M. de Jong, P.V.J.M. Hoogland, R.J.M. Groen, Transient cauda equina compression syndrome and headache caused by internal vertebral venous plexus engorgement in a teenage female with vena cava inferior agenesis and iliac vein thrombosis, J. Neurol. Neurosurg. Psychiatry. 78 (2007) 1283–1284, https://doi.org/10.1136/jnnp.2007.114629.
[11] S. Specchi, M.-A. d'Anjou, E.N. Carmel, G. Bertolini, Computed tomographic characteristics of collateral venous pathways in dogs with caudal vena cava obstruction, Vet. Radiol. Ultrasound. 55 (2014) 531–538, https://doi.org/10.1111/vru.12167.
[12] J.J. Pagani, J.L. Thomas, M.E. Bernardino, Computed tomographic manifestations of abdominal and pelvic venous collaterals, Radiology. 142 (1982) 415–419, https://doi.org/10.1148/radiology.142.2.6459608.
[13] A.H. Sonin, M.J. Mazer, T.A. Powers, Obstruction of the inferior vena cava: a multiple-modality demonstration of causes, manifestations, and collateral pathways, Radiographics. 12 (1992) 309–322, https://doi.org/10.1148/radiographics.12.2.1561419.
[14] W.-Y. Shi, S. Wu, L.-Y. Hu, C.-J. Liu, J.-P. Gu, Swine model of thrombotic caval occlusion created by autologous thrombus injection with assistance of intra-caval net knitting, Sci. Rep. 5 (2015) 18546, https://doi.org/10.1038/srep18546.
[15] J.R. Hetthéssy, A.-M. Tőkés, S. Kérész, P. Balla, G. Dörnyei, E. Monos, G.L. Nádasy, High pressure-low flow remodeling of the rat saphenous vein wall, Phlebology. 33 (2018) 128–137, https://doi.org/10.1177/0268355516688984.
[16] J.A. Diaz, S.K. Wrobleski, C.M. Alvarado, A.E. Hawley, N.K. Doornbos, P.A. Lester,

S.E. Lowe, J.E. Gabriel, K.J. Roelofs, P.K. Henke, R.G. Schaub, T.W. Wakefield, D.D. Myers, P-selectin inhibition therapeutically promotes thrombus resolution and prevents vein wall fibrosis better than enoxaparin and an inhibitor to von Willebrand factor, Arterioscler. Thromb. Vasc. Biol. 35 (2015) 829–837, https://doi.org/10.1161/ATVBAHA.114.304457.

[17] P.A. Araoz, G.P. Reddy, H. Tarnoff, C.L. Roge, C.B. Higgins, MR findings of collateral circulation are more accurate measures of hemodynamic significance than arm-leg blood pressure gradient after repair of coarctation of the aorta, J. Magn. Reson. Imaging. 17 (2003) 177–183, https://doi.org/10.1002/jmri.10238.

[18] S. Pujadas, G.P. Reddy, O. Weber, C. Tan, P. Moore, C.B. Higgins, Phase contrast MR imaging to measure changes in collateral blood flow after stenting of recurrent aortic coarctation: initial experience, J. Magn. Reson. Imaging. 24 (2006) 72–76, https://doi.org/10.1002/jmri.20613.

[19] J.M. Greve, T.J. Chico, H. Goldman, S. Bunting, F. V Peale, A. Daugherty, N. van Bruggen, S.P. Williams, Magnetic resonance angiography reveals therapeutic enlargement of collateral vessels induced by VEGF in a murine model of peripheral arterial disease., J. Magn. Reson. Imaging. 24 (2006) 1124–32. doi:https://doi.org/10.1002/jmri.20731.

[20] M.R. Prince, H.L. Zhang, G.H. Roditi, T. Leiner, W. Kucharczyk, Risk factors for NSF: a literature review, J. Magn. Reson. Imaging. 30 (2009) 1298–1308, https://doi.org/10.1002/jmri.21973.

[21] V.M. Runge, Safety of the gadolinium-based contrast agents for magnetic resonance imaging, focusing in part on their accumulation in the brain and especially the dentate nucleus, Invest. Radiol. 51 (2016) 273–279, https://doi.org/10.1097/RLI.0000000000000273.

[22] R.J. McDonald, D. Levine, J. Weinreb, E. Kanal, M.S. Davenport, J.H. Ellis, P.M. Jacobs, R.E. Lenkinski, K.R. Maravilla, M.R. Prince, H.A. Rowley, M.F. Tweedle, H.Y. Kressel, Gadolinium retention: a research roadmap from the 2018 NIH/ACR/RSNA workshop on gadolinium chelates, Radiology. 289 (2018) 517–534, https://doi.org/10.1148/radiol.2018181151.

[23] D.L. Parker, C. Yuan, D.D. Blatter, MR angiography by multiple thin slab 3D acquisition, Magn. Reson. Med. 17 (1991) 434–451, https://doi.org/10.1002/mrm.1910170215.

[24] R.O. Robison, D.D. Blatter, D.L. Parker, W.W. Barney, D.M. Perry, K.C. Goodrich, Reduction of slab boundary artifact with multiple overlapping thin slab acquisition in MR angiography of the cervical carotid artery, J. Magn. Reson. Imaging. 4 (1994) 529–535, https://doi.org/10.1002/jmri.1880040404.

[25] D. Myers, D. Farris, A. Hawley, S. Wrobleski, A. Chapman, L. Stoolman, R. Knibbs, R. Strieter, T.W. Wakefield, selectins influence thrombosis in a mouse model of experimental deep venous thrombosis, J. Surg. Res. 108 (2002) 212–221, https://doi.org/10.1006/jsre.2002.6552.

[26] B.M. Wojcik, S.K. Wrobleski, A.E. Hawley, T.W. Wakefield, D.D. Myers, J.A. Diaz, Interleukin-6: a potential target for post-thrombotic syndrome, Ann. Vasc. Surg. 25 (2011) 229–239, https://doi.org/10.1016/j.avsg.2010.09.003.

[27] J.A. Diaz, D.M. Farris, S.K. Wrobleski, D.D. Myers, T.W. Wakefield, Inferior vena cava branch variations in C57BL/6 mice have an impact on thrombus size in an IVC ligation (stasis) model, J. Thromb. Haemost. 13 (2015) 660–664, https://doi.org/10.1111/jth.12866.

[28] K.A. Patterson, X. Zhang, S.K. Wrobleski, A.E. Hawley, D.A. Lawrence, T.W. Wakefield, D.D. Myers, J.A. Diaz, Rosuvastatin reduced deep vein thrombosis in ApoE gene deleted mice with hyperlipidemia through non-lipid lowering effects, Thromb. Res. 131 (2013) 268–276, https://doi.org/10.1016/j.thromres.2012.12.006.

[29] E.P. DeRoo, S.K. Wrobleski, E.M. Shea, R.K. Al-Khalil, A.E. Hawley, P.K. Henke, D.D. Myers, T.W. Wakefield, J.A. Diaz, The role of galectin-3 and galectin-3-binding protein in venous thrombosis, Blood. 125 (2015) 1813–1821, https://doi.org/10.1182/blood-2014-04-569939.

[30] J.A. Diaz, S.K. Wrobleski, A.E. Hawley, B.R. Lucchesi, T.W. Wakefield, D.D. Myers, Electrolytic inferior vena cava model (EIM) of venous thrombosis., J. Vis. Exp. (2011) e2737. doi:https://doi.org/10.3791/2737.

[31] J.A. Diaz, C.M. Alvarado, S.K. Wrobleski, D.W. Slack, A.E. Hawley, D.M. Farris, P.K. Henke, T.W. Wakefield, D.D. Myers, The electrolytic inferior vena cava model (EIM) to study thrombogenesis and thrombus resolution with continuous blood flow in the mouse, Thromb. Haemost. 109 (2013) 1158–1169, https://doi.org/10.1160/TH12-09-0711.

[32] J.A. Diaz, A.E. Hawley, C.M. Alvarado, A.M. Berguer, N.K. Baker, S.K. Wrobleski, T. W. Wakefield, B.R. Lucchesi, D.D. Myers, Thrombogenesis with continuous blood flow in the inferior vena cava. A novel mouse model., Thromb. Haemost. 104 (2010) 366–75. doi:https://doi.org/10.1160/TH09-09-0672.

[33] O.R. Palmer, M.E. Shaydakov, J.P. Rainey, D.A. Lawrence, J.M. Greve, J.A. Diaz, Update on the electrolytic IVC model for pre-clinical studies of venous thrombosis, Res. Pract. Thromb. Haemost. 2 (2018) 266–273, https://doi.org/10.1002/rth2.12074.

[34] J.A. Diaz, P. Saha, B. Cooley, O.R. Palmer, S.P. Grover, N. Mackman, T.W. Wakefield, P.K. Henke, A. Smith, B.K. Lal, Choosing a mouse model of venous thrombosis, Arterioscler. Thromb. Vasc. Biol. 39 (2019) 311–318, https://doi.org/10.1161/ATVBAHA.118.311818.

[35] G.A. Hish, J.A. Diaz, A.E. Hawley, D.D. Myers, P.A. Lester, Effects of analgesic use on inflammation and hematology in a murine model of venous thrombosis, J. Am. Assoc. Lab. Anim. Sci. 53 (2014) 485–493 http://www.pubmedcentral.nih.gov/articlerender.fcgi?artid=4181690&tool=pmcentrez&rendertype=abstract , Accessed date: 30 May 2016.

[36] M. Ackermann, M.A. Konerding, Vascular casting for the study of vascular morphogenesis, Methods Mol. Biol. 1214 (2015) 49–66, https://doi.org/10.1007/978-1-4939-1462-3_5.

[37] C.M. Alvarado, J.A. Diaz, A.E. Hawley, S.K. Wrobleski, R.E. Sigler, D.D. Myers, Male mice have increased thrombotic potential: sex differences in a mouse model of venous thrombosis, Thromb. Res. 127 (2011) 478–486, https://doi.org/10.1016/j.thromres.2011.01.004.